

# Transient Three Dimensional FE Modeling for Thermal Analysis of Pulsed Current Gas Tungsten Arc Welding of Aluminum Alloy

N. Karunakaran, V. Balasubramanian

**Abstract**—This paper presents the results of a study aimed at establishing the temperature distribution during the welding of aluminum alloy plates by Pulsed Current Gas Tungsten Arc Welding (PCGTAW) and Constant Current Gas Tungsten Arc Welding (CCGTAW) processes. Pulsing of the GTA welding current influences the dimensions and solidification rate of the fused zone, it also reduces the weld pool volume hence a narrower bead. In this investigation, the base material considered was aluminum alloy AA 6351 T6, which is finding use in aircraft, automobile and high-speed train components. A finite element analysis was carried out using ANSYS, and the results of the FEA were compared with the experimental results. It is evident from the study that the finite element analysis using ANSYS can be effectively used to model PCGTAW process for finding temperature distribution.

**Keywords**—Gas tungsten arc welding, pulsed current, finite element analysis, thermal analysis, aluminum alloy.

## I. INTRODUCTION

WELD fusion zones typically exhibit coarse columnar grains because of the prevailing thermal conditions during weld metal solidification. This often results in inferior weld mechanical properties and poor resistance to hot cracking. It is thus highly desirable to control solidification structure in welds; such control is often very difficult because of the higher temperatures and higher thermal gradients in welds in relation to castings and the epitaxial nature of the growth process. Nevertheless, several methods for refining weld fusion zones have been tried.

Two relatively new techniques, current pulsing and magnetic arc oscillation have gained popularity because of their striking promise and the relative ease with which these techniques can be applied to actual industrial situations with only minor modifications to the existing welding equipment [1].

Pulsed current welding, developed in 1950s, is a variation of constant current welding which involves cycling of the welding current from a high level to a low level at a selected regular frequency.

The high level of the peak current is generally selected to give adequate penetration and bead contour, while the low

level of the background current is set at a level sufficient to maintain a stable arc. This permits arc energy to be used efficiently to fuse a spot of controlled dimensions in a short time producing the weld as a series of overlapping nuggets and limits the wastage of heat by conduction into the adjacent parent material as in normal constant current welding. The technique has secured a niche for itself in specific applications such as in welding of root passes of tubes, and in welding thin plates, where precise control over penetration and heat input are required to avoid burn through [2].

Current pulsing has been used by few investigators [3]-[5] to obtain grain refinement in weld fusion zones and improvement in weld mechanical properties. Most of the reported literatures have focused on pulsed current welding and their effects on mechanical and metallurgical properties and no literature is available on thermal analysis of PCGTAW process. Hence, the present investigation has been carried out to understand the effect of pulsed current welding technique on temperature distribution in AA 6351 T6 aluminum alloy using finite element analysis.

The basic theory of heat flow developed by Fourier and applied to moving heat sources by Rosenthal in the late 1930s is still the most popular analytical method for calculating the thermal history of welds. As many researchers have shown [6]-[9], Rosenthal's analysis (which assumes a point, line, or plane source of heat) is subject to serious error for temperatures in or near the fusion and heat-affected zones. Since Rosenthal's point or line models assume that the flux and temperature is infinite at the source, it would not account for the actual distribution of the heat in the arc and hence would not accurately predict temperatures near the arc. Then Pavelic [7] suggested that the heat source should be distributed and he proposed a Gaussian distribution of flux deposited on the surface of the work piece. Further John Goldak [9] proposed in his investigation a 'double ellipsoid' configuration of the heat source. Many other investigators have used this heat source model [10], [11]. The present investigation has been carried out to understand the effect of pulsed current welding technique on temperature distribution in AA 6351 T6 aluminum alloy with the general purpose Finite Element Analysis code ANSYS. The heat source model considered here is of the double ellipsoid configuration.

## II. EXPERIMENTAL WORK

In this investigation, plates of 4mm thick were used as base material. The chemical composition and mechanical properties

N. Karunakaran is Associate Professor in the Department of Mechanical Engineering, Annamalai University, Annamalai Nagar, Tamilnadu, India (Phone: +919443405920; e-mail: cdl.karun28@gmail.com).

V. Balasubramanian is Professor in the Department of Manufacturing Engineering, Annamalai University, Annamalai Nagar, Tamilnadu, India. (e-mail: visvabalu@yahoo.com).

of base metal are presented in Table I. The plates of aluminum alloy were cut to the required size (150 x 150mm) by power hacksaw cutting and grinding. Square butt joint configuration was used to fabricate the welded joints. Single pass, autogenous welding procedure (without filler metal addition) was applied to fabricate the joints. High purity (99.99%) argon gas was used as shielding gas with a flow rate of 9 lpm [12]. 2% thoriated tungsten electrode of 3.2 mm diameter was used with DC straight polarity (electrode -ve and weld plate +ve) to carry out the experiments. The arc length was maintained at 2mm.

TABLE I (A)  
CHEMICAL COMPOSITION (WT %) OF BASE METAL

Mg	Si	Fe	Cu	Mn	Zn	Zr	Al
0.7	1.2	0.5	0.1	0.6	0.2	0.05	Remainder

TABLE I (B)  
MECHANICAL PROPERTIES OF BASE METAL

Yield Strength (MPa)	Tensile Strength (MPa)	Elongation in 50 mm gauge length (%)	Micro Hardness at 0.05 Kg load (Hv)
150	250	20	95

The experimental setup is shown in Fig. 1. The Lincoln Electric GTA welding machine controlled the welding parameters, (model: "Precision TIG 375"). To measure the temperature during welding the K Type Chromel – Alumel thermocouple was used [13]-[15]. The hot end diameter of the thermocouple was 1.5mm, the cold end was fixed to a thermocouple bank and this was in turn connected to the data acquisition system (DAQ) Labview [16]. Labview was a bundled package on virtual instrumentation having the flexibility to measure the parameter of concern at very short interval. When used on DC straight polarity Labview acquired data for both heating and cooling, but in AC configuration the DAQ could acquire data only after the welding time, hence providing temperature history for the cooling. This being the limitation the DC straight polarity was used for the investigation. Fig. 2 shows the positions on the plate where the thermocouples were glued to a depth of 2mm, the holes were drilled at the bottom of the plate [17]. The data acquisition system of LABVIEW was used to acquire the temperature every second [18] during weld from these 3 locations as well as the room temperature. It is seen from Lu, and Kou, [19] that for the GTAW welding process, the molten surface is turbulent if the welding current is more than 225 amps hence limited to this value.



Fig. 1 Experimental setup

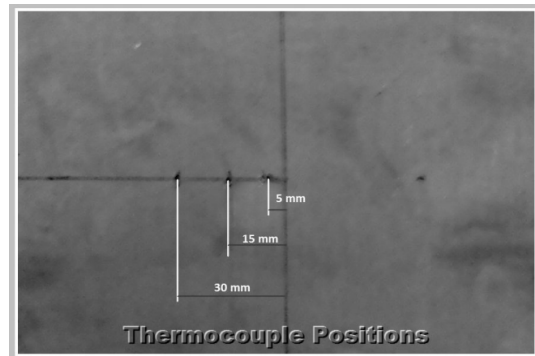
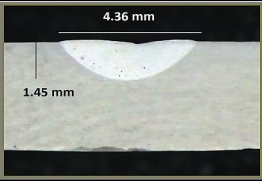
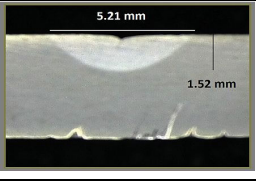


Fig. 2 Thermocouple positions

Before welding was performed, the plates were cleaned and thermocouples were incorporated in its appropriate positions. Welding was done by both the constant current (CC) and the pulsed current (PC) process. A number of trial runs on the base material were performed to fix the upper and lower heat input levels. For the CC process higher than 294 J/mm (140 amps) resulted in burning of base metal and in PC process the burning happened above 269 J/mm (160 amps). The various penetrations that were achieved during welding were compared. From the comparison the joint fabricated at 256J/mm (120 amps) in constant current had a penetration of 1.45mm that was in parance with the joint welded at 232J/mm (140 amps) of pulsed current whose penetration was 1.52 mm. The ratio of penetration to plate thickness was 0.36 and 0.38 for constant current and pulsed current respectively. The ratio of width to penetration was 3 and 3.43 for constant current and pulsed current respectively. Hence these two joints exhibited similar physical characteristics and amenable for comparison as shown in Table II.

TABLE II  
BEAD PROFILE

Current (amps)	Constant Current (CC)	Current (amps)	Pulsed Current (PC)	*P/T		W/P*	
				CC	PC	CC	PC
120		140		0.36	0.38	3	3.43

\*P: depth of penetration; W: width of the weld bead; T: plate thickness

TABLE III (A)  
PULSED CURRENT WELDING PARAMETER

Peak Current (amps)	Base Current (amps)	Voltage (volts)	Pulse on time (%)	Frequency (hz)	Welding speed (mm/sec)	Efficiency (%)	Heat Input during peak current (J/mm)	Heat Input during base current (J/mm)
140	70	12.5	50	6	4.167	70	294	147

TABLE III (B)  
CONSTANT CURRENT WELDING PARAMETER

Current (amps)	Voltage (volts)	Welding speed (mm/sec)	Efficiency (%)	Heat Input (Joules/mm)
120	12.7	4.167	70	256

The process parameter of these two joints is shown in Table III. For the calculation of the heat Input (Q) the relationship used for constant current process was  $Q = \{(V \times I) / n\} \eta$  where V is the voltage, I is the current, n is the welding speed and  $\eta$  is the efficiency of utilization of the heat generated [17, 20].

The calculation of heat input (Q) for the pulsed current process was done by first computing the mean current using the relationship  $I_m = \{(I_p \times t_p) + (I_b \times t_b)\} / tT$ . Where  $I_m$  is the mean current  $I_p$  is the peak current  $I_b$  is the base current  $t_p$  is the time on peak pulse  $t_b$  is the time on base current  $tT$  is the total time [20], [23]. From this the RMS value of current or the effective current was computed and the heat input values obtained. For the calculation of the heat Input (Q) the relationship used for constant current process was  $Q = \{(V \times I) / n\} \eta$  where V is the voltage, I is the current, n is the welding speed and  $\eta$  is the efficiency of utilization of the heat generated [17], [20].

To calculate the heat input at peak and base current the above formula was used. The process parameter of these two joints is shown in Table III. For the modeling purpose the heat input was calculated for the peak current and the base current and presented in Table III (A) [21]–[24].

### III. MODELING DISCUSSION

An axisymmetric three-dimensional transient model is proposed with the general-purpose Finite Element Analysis code ANSYS. The governing equation [25], [26] for heat transfer in three dimensions arrived from the Helmholtz equation is

$$\frac{\partial}{\partial x} \left( k_x \frac{\partial T}{\partial x} \right) + \frac{\partial}{\partial y} \left( k_y \frac{\partial T}{\partial y} \right) + \frac{\partial}{\partial z} \left( k_z \frac{\partial T}{\partial z} \right) + Q = 0 \quad (1)$$

where  $k_x$ ,  $k_y$  and  $k_z$  are the thermal conductivities in the x, y and z directions and Q is the internal heat generation

The derivation for the nodes and elements are done for the steady state conditions and transformed to the transient conditions. In the three dimensional analysis only conduction effects are included, the convection effects are treated most efficiently as boundary conditions

The domain to which (1) applies is represented by a mesh of finite elements in which the temperature distribution is discretized as

$$T(x, y, z) = \sum_{i=1}^M N_i(x, y, z) T_i = \{N\} \{T\} \quad (2)$$

where  $N_i(x, y, z)$  is the interpolation function associated with nodal temperature  $T_i$ ,  $\{N\}$  is the row matrix of interpolation functions, and  $\{T\}$  is the column matrix (vector) of nodal temperatures, and M is the number of nodes per element. Application of the Galerkin method to (1) results in M residual equations.

The volume integral formally gives the element stiffness matrix

$$\iiint_V \left[ \frac{\partial}{\partial x} \left( K_x \frac{\partial T}{\partial x} \right) + \frac{\partial}{\partial y} \left( K_y \frac{\partial T}{\partial y} \right) + \frac{\partial}{\partial z} \left( K_z \frac{\partial T}{\partial z} \right) + Q \right] N_i dV = 0 \quad (3)$$

where,  $i = 1, \dots, M$  and V is element volume.

The derivative terms can be written as follows

$$\begin{aligned} \frac{\partial}{\partial x} \left( K_x \frac{\partial T}{\partial x} \right) N_i &= \frac{\partial}{\partial x} \left( K_x \frac{\partial T}{\partial x} N_i \right) - K_x \frac{\partial T}{\partial x} \frac{\partial N_i}{\partial x} \\ \frac{\partial}{\partial y} \left( K_y \frac{\partial T}{\partial y} \right) N_i &= \frac{\partial}{\partial y} \left( K_y \frac{\partial T}{\partial y} N_i \right) - K_y \frac{\partial T}{\partial y} \frac{\partial N_i}{\partial y} \\ \frac{\partial}{\partial z} \left( K_z \frac{\partial T}{\partial z} \right) N_i &= \frac{\partial}{\partial z} \left( K_z \frac{\partial T}{\partial z} N_i \right) - K_z \frac{\partial T}{\partial z} \frac{\partial N_i}{\partial z} \end{aligned} \quad (4)$$

the residual equations become

$$\iiint_V \left[ \frac{\partial}{\partial x} (K_x \frac{\partial T}{\partial x} Ni) + \frac{\partial}{\partial y} (K_y \frac{\partial T}{\partial y} Ni) + \frac{\partial}{\partial z} (K_z \frac{\partial T}{\partial z} Ni) \right] dv + \iiint_V Q Ni dv$$

$$= \iiint_V \left[ K_x \frac{\partial T}{\partial x} \frac{\partial Ni}{\partial x} + K_y \frac{\partial T}{\partial y} \frac{\partial Ni}{\partial y} + K_z \frac{\partial T}{\partial z} \frac{\partial Ni}{\partial z} \right] dv - (i=1, \dots, M) \quad (5)$$

The integral on the left side of (5) contains a perfect differential in three dimensions and can be replaced by an integral over the surface of the volume using Green's theorem in three dimensions.

The Green-Gauss theorem (also known as Green's theorem in the plane) stated as follows: Let  $F(x, y, z)$ ,  $G(x, y, z)$  and  $H(x, y, z)$  be continuous functions defined in a region of the xyz space (the element volume in our context), then  $F = kx (\partial T / \partial x)$ ,  $G = ky (\partial T / \partial y)$  and  $H = kz (\partial T / \partial z)$

$$\iiint_V \left( \frac{\partial F}{\partial x} + \frac{\partial G}{\partial y} + \frac{\partial H}{\partial z} \right) dv = \iint_A (F n_x + G n_y + H n_z) \quad (6)$$

where A is the surface area of the volume and  $n_x, n_y, n_z$  are the Cartesian components of the outward unit normal vector of the surface area.

Invoking Fourier's law  $\{q_x = kx (\partial T / \partial x), q_y = ky (\partial T / \partial y), q_z = kz (\partial T / \partial z)$  and comparing (5) to the first term of (6), we have

$$-\iint_A (q_x n_x + q_y n_y + q_z n_z) Ni dA + \iiint_V Q Ni dV$$

$$= \iiint_V \left[ K_x \frac{\partial T}{\partial x} \frac{\partial Ni}{\partial x} + K_y \frac{\partial T}{\partial y} \frac{\partial Ni}{\partial y} + K_z \frac{\partial T}{\partial z} \frac{\partial Ni}{\partial z} \right] dv - (i=1, \dots, M) \quad (7)$$

Inserting the matrix form of (2) and rearranging, we have

$$\iiint_V \left[ K_x \frac{\partial [N]}{\partial x} \frac{\partial Ni}{\partial x} + K_y \frac{\partial [N]}{\partial y} \frac{\partial Ni}{\partial y} + K_z \frac{\partial [N]}{\partial z} \frac{\partial Ni}{\partial z} \right] \{T\} dV$$

$$= \iiint_V Q Ni dV - \iint_A (q_x n_x + q_y n_y + q_z n_z) Ni dA (i=1, \dots, M) \quad (8)$$

Equation (8) represents a system of M algebraic equations in the M unknown nodal temperatures  $\{T\}$ . With the exception that convection effects are not included here. In matrix notation, the system of equations for the three dimensional element formulations is

$$= \iiint_V Q Ni dV - \iint_A (q_x n_x + q_y n_y + q_z n_z) Ni dA (i=1, \dots, M) \quad (9)$$

and (7) is in the desired form

$$\left\{ T^{(e)} \right\} + [K^{(e)}] = \left\{ f_Q^{(e)} \right\} + \left\{ f_q^{(e)} \right\} \quad (10)$$

Comparing the last two equations, the element conductance (stiffness) matrix is

$$[K^{(e)}] = \iiint_V \left[ K_x \frac{\partial [N]^T}{\partial x} \frac{\partial [N]}{\partial x} + K_y \frac{\partial [N]^T}{\partial y} \frac{\partial [N]}{\partial y} + K_z \frac{\partial [N]^T}{\partial z} \frac{\partial [N]}{\partial z} \right] dV \quad (11)$$

the element force vector representing internal heat generation is

$$\{f_Q^{(e)}\} = \iiint_V Q [N]^T dV \quad (12)$$

and the element nodal force vector associated with heat flux across the element surface area is

$$\{f_q^{(e)}\} = -\iint_A (q_x n_x + q_y n_y + q_z n_z) [N]^T dA \quad (13)$$

The model assembly procedure for a transient heat transfer problem is the same as for a steady-state problem, with the notable exception that we must also assemble a global capacitance matrix. Element nodes are assigned to global nodes and the element capacitance matrix terms are added to the appropriate global positions in the global capacitance matrix, as with the conductance matrix terms.

The conditions for the transient state are derived out of steady state by the addition of the capacitance matrix. Thus for the element

$$[C^{(e)}] \left\{ T^{(e)} \right\} + [K^{(e)}] \left\{ T^{(e)} \right\} = \left\{ f_Q^{(e)} \right\} + \left\{ f_q^{(e)} \right\} \quad (14)$$

where  $[C^{(e)}]$  is the element capacitance matrix defined by in the x direction

$$[C^{(e)}] = c \rho A \int_{x_1}^{x_2} \int_{N_1}^{N_2} [N_1 \ N_2] dx = c \rho A \int_{x_1}^{x_2} [N]^T N dx \quad (15)$$

Hence, on system assembly, we obtain the global equations

$$[C] \{T\} + [K] \{T\} = \{FQ\} + \{Fq\} \quad (16)$$

where the gradient force vector  $\{Fq\}$  is composed of either unknown heat flux values to be determined or convection terms to be equilibrated with the flux at a boundary node.

The 3 D element of "SOLID Brick 8 node 70" was chosen for the analysis. Half sheet was modeled since the other half would be symmetrical. Mapped meshing was used for the model, by defining the nodes. Finer meshing was done for the near weld zone while coarse meshing on the other areas [27]. The aspect ratio for finer mesh was 5.99 and coarser mesh was 8.98, 11.98 & 14.97 – well below the limit of 20. The model for Pulsed current was designed based on the parameter of current [21]–[23]. For a frequency of 6Hz, Pulse On Time 50% and for a speed of 4.167 mm/sec yielded

- Number of Pulse per mm – 1.434
- Time taken to traverse 1mm – 0.239 Sec
- Number of load steps per mm - 3

Time per Load step - 0.0797 Sec  
 Distance per Load step - 0.333mm

The details of the model are presented in Table IV.

TABLE IV  
 MODEL DETAILS

Process	Nodes	Elements	Width of weld (mm)	Size of Plate (mm)	Emissivity	Convection H T Coeff (Watts/m <sup>2</sup> K)	Lumped HT Coeff (Watts/m <sup>2</sup> K)
Pulsed Current	96965	75600	5.2	150 x 150 x 4	0.09	20	2.191
Constant Current	64715	50400	4.4				

For the constant current one load step for 0.5mm was considered and the time for each load step was 0.1195 secs. The measured width of the weld is shown in Table IV.

The temperature dependent Properties of thermal conductivity, specific heat and density were given as input. (Fig. 3) [6], [11], [17], [20]. Subroutines were written in APDL (ANSYS Parametric Design Language) using the DO loop and IF for the pulsing of heat input.

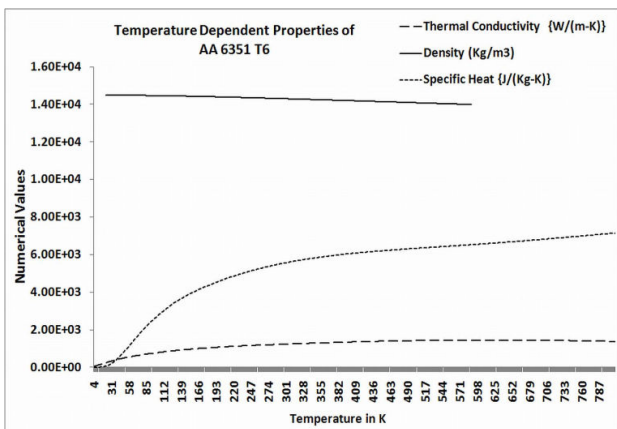
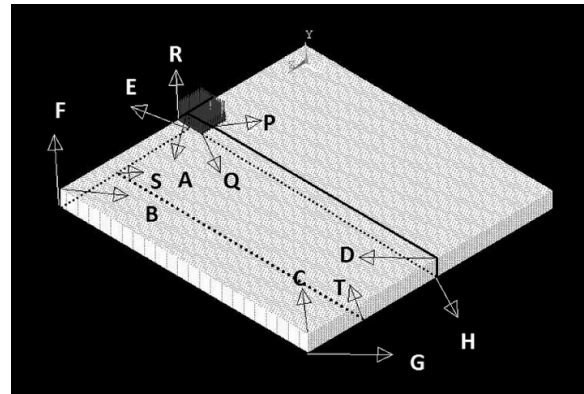


Fig. 3 Temperature dependent properties of AA6351 T6

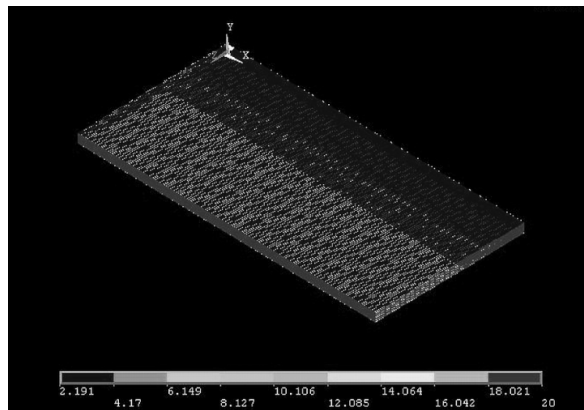
A. Boundary Conditions

In the case of three-dimensional heat transfer, four types of boundary conditions have to be specified: (a) specified temperatures, (b) specified heat flux, (c) convection conditions and (d) radiation conditions.

The first case, specified temperatures, is taken into account in the usual manner, by reducing the system equations by simply substituting the known nodal temperatures into the system equations. For the others the conditions are defined in zones. For the Zones: (as shown in Fig. 4)



(a)



(b)

Fig. 4 (a) Boundary Conditions (b) Boundary conditions as applied to the model

APQR - The heat flux specified to the surface elements.

ARQPDCB; STHE - The temperature dependent convection and radiation coefficients is applied to this boundary. For the radiation and convection boundary conditions, a combined heat transfer coefficient was calculated from the relationship:

$$H = 24.1 \times 10^{-4} \epsilon T^{1.61} \tag{17}$$

where E is the emissivity or degree of blackness of the surface of the body.

ABFE; BCGF; CDHG - The outer areas are subjected to convection conditions. For such convection boundary conditions, the flux conditions must be in balance with the convection from the area of concern.

STGF - This is the Insulated Part on the bottom of plate hence adiabatic conditions specified.

ADHE - For the symmetrical edge adiabatic boundary condition.

*B. Heat Source Model*

The ellipsoidal heat source model revealed that the temperature gradient in front of the heat source was not as steep as expected and the gentler gradient at the trailing edge of the molten pool was steeper than experimental measurements [9]–[11]. Hence two ellipsoidal sources were combined as shown in Fig. 5. The front half of the source is the quadrant of one ellipsoidal source, and the rear half is the quadrant of another ellipsoid. The estimation of the heat input was made based on (18) and (19) [11]:

$$q_r = \frac{6\sqrt{3}Qf_r}{\pi\sqrt{a_rbc}} \exp\left(-3\left[\frac{x^2}{a_r^2} + \frac{y^2}{b^2} + \frac{z^2}{c^2}\right]\right) \quad (18)$$

$$q_f = \frac{6\sqrt{3}Qf_f}{\pi\sqrt{a_fbc}} \exp\left(-3\left[\frac{x^2}{a_f^2} + \frac{y^2}{b^2} + \frac{z^2}{c^2}\right]\right) \quad (19)$$

where  $f_f$  and  $f_r$  are the frontal and rear fraction of the heat flux,  $a_f, a_r, b$  and  $c$  are the parametric values obtained from the metallographic data and from weld pool surface ripple markings as depicted in Fig. 5.  $Q$  is the calculated heat input.

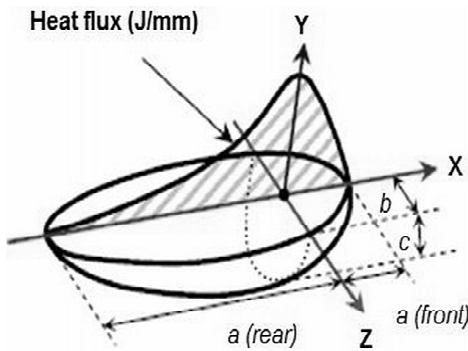


Fig. 5 Heat Input Model

The  $q_r$  and  $q_f$  values were given as input to the model by a subroutine created by the APDL.

*C. Phase Change*

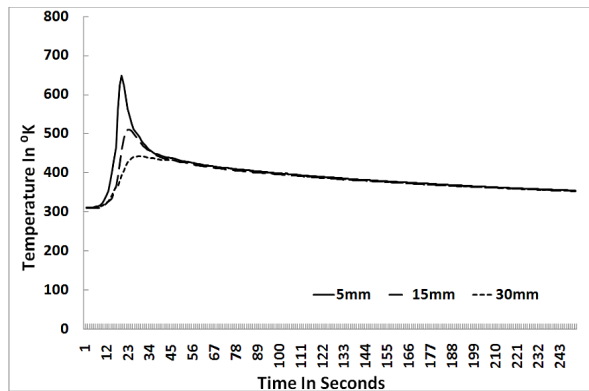
To analyze the phase change problem, in the nonlinear transient thermal analysis the latent heat was accounted for (heat stored or released during a phase change). To account for latent heat, the enthalpy of the material as a function of temperature was defined. Hence the latent heat effect (accompanying change in phase from liquid to solid), is approximated by specifying a rapid variation in enthalpy over the “mushy” zone in a temperature range of  $\Delta T$ . The enthalpy ( $h$ ) variation is computed from (20) and given as input [28] by the APDL subroutine.

$$h = \int \rho c(T) dT \quad (20)$$

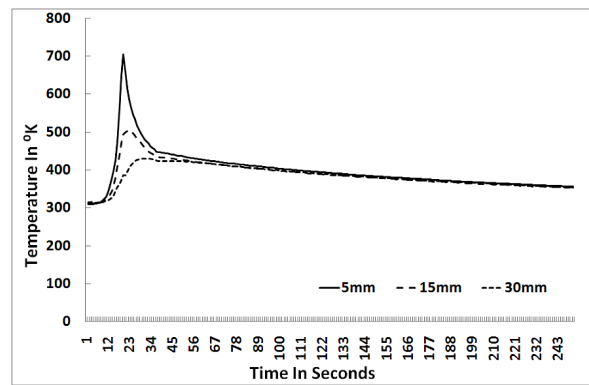
IV. RESULTS AND DISCUSSION

*A. Temperature Profile*

The parameters defined in the model were executed and the plots of time versus temperature were obtained. Figs. 6 (a), (b) shows the plot obtained from the experimental results for constant current and pulsed current respectively for heating and cooling. It is seen that the peak temperature attained by the constant current process was 648 K and that of pulsed current 704 K for the 5mm distance from the weld centre. The model was run for 36 seconds and the heating curves were plotted for the 5mm and 15mm from weld centre, The temperature profile for the modeled values and the experimental values are shown in Figs. 7 (a), (b) for the pulsed current and Figs. 8 (a), (b) for the constant current.

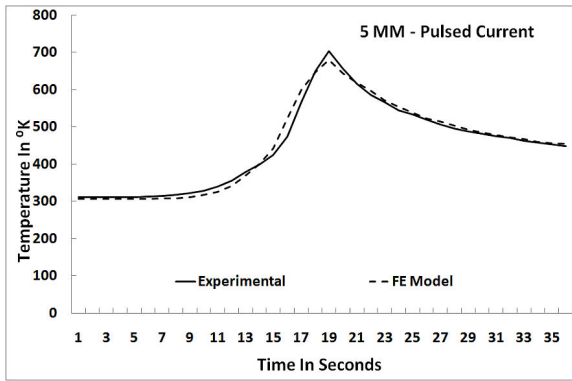


(a)

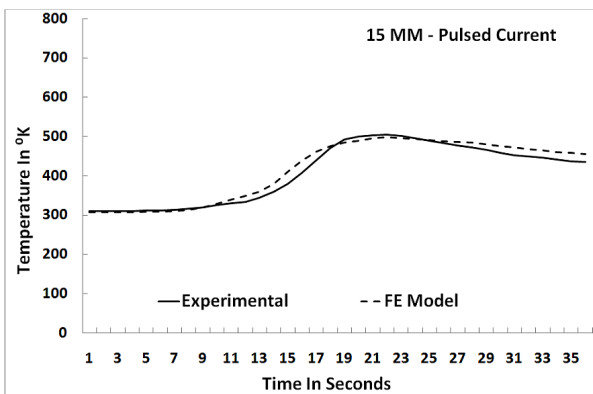


(b)

Fig. 6 (a) Constant Current Temperature profile (b) Pulsed Current Temperature profile

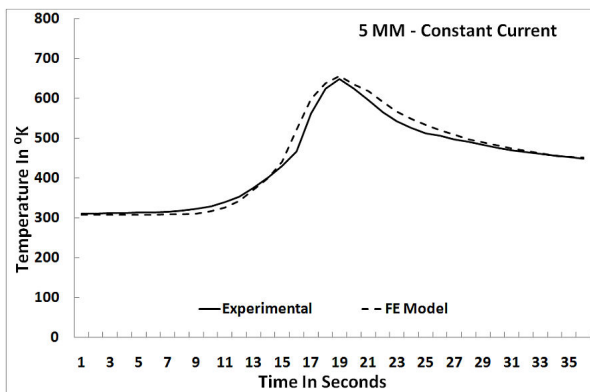


(a)

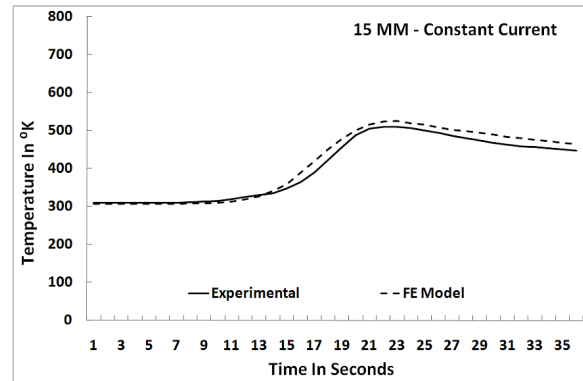


(b)

Fig. 7 (a) Experimental Vs FEA at 5 mm Pulsed Current (b) Experimental Vs FEA at 15 mm Pulsed Current



(a)



(b)

Fig. 8 (a) Experimental Vs FEA at 5 mm Constant Current (b) Experimental Vs FEA at 15 mm Constant Current

It was seen from the plots that the ANSYS FEA model was in agreement with the experimental values. In the case of 5mm the results of FEA were very close to that of the experimental values, the reason for this can be attributed to the consideration of the phase change in the model as well as the pulsing of heat input between the peak and the base current. The profile curves by the model showed that for pulsed current the modeled values on heating and cooling were above the experimental values. In pulsed current profiles, it is seen that after the peak temperature is reached the values are more or less the same as that of the experimental values. This can be attributed to the thermal properties of the material. The profile curves by the model when compared to that of the experimental was below 10% deviation. The bead profile of the pulsed current were more controlled and the effect of the surface tension and buoyancy forces are seen clearly in both the profiles of constant current and pulsed current. The cooling rate for constant current is  $14.4^{\circ}\text{C}/\text{second}$  and for pulsed current it was  $12.9^{\circ}\text{C}/\text{second}$

#### B. Prediction of Temperature at Weld Centre

From the computed results, the temperature at the weld centre for both the pulsed and constant current was plotted. Fig. 9 shows the values of the same It is seen that the peak temperature of the pulsed current was more than that of constant current, during the initial heating process the temperature of the pulsed current was lower but as the temperature rose to the melting point the temperature of pulsed current was higher. The predicted peak temperature of the constant current process was 1262K and the pulsed current process was 1301K. The material was in molten state for 12 seconds and 13 seconds for the constant current and pulsed current process respectively.

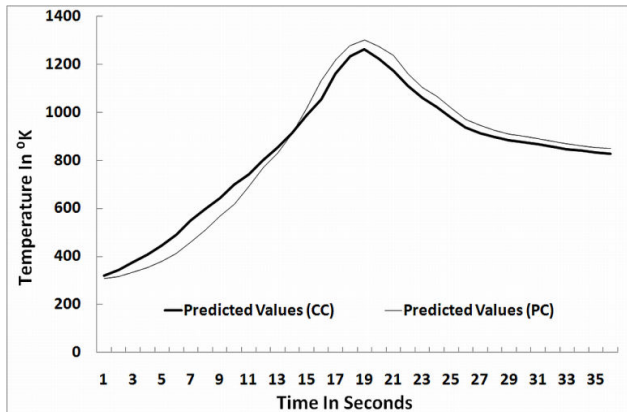


Fig. 9 Predicted values of temperature at weld centre

### V. CONCLUSION

From this investigation, it was found that

1. The predicted values of temperature using the transient three dimensional FEA model are in good agreement with the experimental values.
2. The incorporation of the pulsing effect by providing two different heat inputs and the double ellipsoid model for the heat source has given realistic results with the phase change consideration.
3. A realistic prediction of the temperature at the weld centre was obtained.

### ACKNOWLEDGMENT

The authors wish to express their sincere thanks to the, Department of Manufacturing Engineering, Annamalai University, Annamalai Nagar 608002 for the facilities provided to carry out this investigation.

### REFERENCES

- [1] Davies CJ and JG Garland. Solidification structures and properties of fusion welds. *Int. Mater. Review*, Vol 20, (1975), 83-106.
- [2] T. Senthil Kumar, V. Balasubramanian, S. Babu and M. Y. Sanavullah, - Effect of pulsed current GTA welding parameters on the fusion zone microstructure of AA6061 aluminum alloy, *Metals and Materials International*, Vol.13, No.4, (2007): 345-351.
- [3] Kou S and Y.Le - Nucleation mechanism and grain refining of weld metal, *Welding Journal*, Vol 65, (1986), 305s – 313s.
- [4] Madhusudhan Reddy G, Gokhale A.A and Prasad Rao K - Optimization of pulse frequency in pulsed current gas tungsten arc welding of aluminium – lithium alloy sheets, *Journal of Material Science & Technology*, Vol. 14, (1998), 61-66
- [5] Potluri N.B, Ghosh P.K, Gupta P.C and Reddy Y.S - Studies on weld metal characteristics and their influences on tensile and fatigue properties of pulsed current GMA welded Al-Zn-Mg alloy, *Welding Research Supplement*, Vol 75, (1996), 62s-70s.
- [6] John Goldak, Aditya Chakravarthi and Malcolm Bibby - A New Finite Element Model for Welding Heat Sources, *Metallurgical Transactions B*, Vol 15B, (1984), 299.
- [7] V. Pavelic, R. Tanbakuchi, O. A. Uyehara, and P. S. Myers: - Experimental and Computed Temperature Histories in Gas Tungsten Arc Welding of Thin Plates, *Welding Journal Research Supplement*, Vol. 48, (1969), 295s-305s.
- [8] R.T.C. Choo, J. Szekeley, R.C. Westhoff, On the calculation of the free surface temperature of gas-tungsten-arc weld pools from first principles: Part I. Modeling the welding arc, *Metallurgical Transactions B*. Vol.23, (1992), 357–369.
- [9] John Goldak, Malcolm Bibby, J. Moore, R. House, and B. Patel, Computer Modeling of heat flow in welds: *Metallurgical Transactions B*, Vol 17B, (1986), 587-600
- [10] X. Shan, C.M. Davies, T. Wangsdan, N.P. O'Dowd, K.M. Nikbin, Thermo-mechanical modelling of a single-bead-on-plate weld using the finite element method *International Journal of Pressure Vessels and Piping*, Vol 86, (2009), 110–121
- [11] Afzaal M. Malik, Ejaz M. Qureshi, Naeem Ullah Dar, Iqbal Khan Analysis of circumferentially arc welded thin-walled cylinders to investigate the residual stress fields *Thin-Walled Structures*, Vol 46, (2008), 1391–1401.
- [12] Balasubramanian, V, V. Ravisankar and G. Madhusudhan Reddy, "Effect of pulsed current welding on mechanical properties of high strength aluminium alloys", *International Journal of Advanced Manufacturing Technology*, Vol.36, (2007), 254-262.
- [13] Sadek C, Absi Alfaro, K S Chawla & John Norrish - Computer Based Data Acquisition for welding research and production, *Journal of Materials Processing Technology*, Vol 53, (1995), 1-13
- [14] Peter R.N. Childs "Practical Temperature Measurements" Elsevier Publications. 1998
- [15] M. Sunar, B.S. Yilbas, K. Boran - Thermal and stress analysis of a sheet metal in welding, *Journal of Materials Processing Technology*, Vol 172, (2006), 123–129.
- [16] Klobcar, D, J. Tusek, B. Taljat "Finite element modeling of GTA weld surfacing applied to hot-work tooling", *Computational Materials Science* 2004 Vol 31, 368–378.
- [17] C.V. Goncalves, L.O. Vilarinho, A. Scotti, G. Guimaraes Estimation of heat source and thermal efficiency in GTAW process by using inverse techniques *Journal of Materials Processing Technology* Vol 172, (2006), 42–51.
- [18] Paul Scott, "Selecting a welding frequency" article at <http://www.thermatool.com/>. 20.04.2010.
- [19] Lu, M., Kou, S., Power and current distribution in Gas Tungsten Arcs. *Welding Journal*, Vol 67(2), (1988), 29s–33s.
- [20] W. H. Kim, S. J. Na - Heat and fluid flow in pulsed current GTA weld pool, *International Journal of Heat and Mass Transfer*, Vol 41, (1998), 3213-3227
- [21] Anuj Chaudhri, Masood Parang, B.E. Nelson Computer simulation and experimental verification of welding in thin steel sheet containment, *International Journal of Heat and Mass Transfer*, Vol 50, (2007), 4439–4445.
- [22] Mohandas T and Madhusudhana Reddy G Effect of frequency of pulsing in gas tungsten arc welding on the microstructure and mechanical properties of titanium alloy welds, *Jl. of Mater Sci Letters*, Vol. 15, (1996), 626-628.
- [23] H.G. Fan, Y.W. Shi, S.J. Na - Numerical analysis of the arc in pulsed current gas tungsten arc welding using a boundary-fitted coordinate, *Journal of Materials Processing Technology* Vol 72, (1997), 437–445.
- [24] V. Ravisankar and V. Balasubramanian, Optimising the pulsed TIG welding parameters to refine the fusion zone, *Science and Technology of Welding & Joining*, Vol.11, No.6, (2006), 112-116.
- [25] Komanduri, R and Z.B. Hou "Thermal Analysis of the Arc Welding Process: Part I. General Solutions" *Metallurgical and Materials Transactions B*, Vol 31B, (2000), 1353-1370
- [26] Little G.H., A.G. Kamtekar "The effect of thermal properties and weld efficiency on transient temperatures during welding" *Computers and Structures*, Vol 68, (1998), 157-165
- [27] Duranton, P, J. Devaux, V. Robin, P. Gilles, J.M. Bergheau "3D modelling of multipass welding of a 316L stainless steel pipe" *Journal of Materials Processing Technology* Vol 153–154, (2004), 457–463
- [28] Andrea Capriccioli, Paolo Frosi "Multipurpose ANSYS FE procedure for welding processes simulation" *Fusion Engineering and Design*, Vol 84, (2009), 546–553.